A&A manuscript no.
(will be inserted by hand later)

Your thesaurus codes are:
06 (08.16.7 Crab, Geminga; 13.07.2)

ASTRONOMY AND ASTROPHYSICS

Phase-resolved TeV Gamma-Ray Characteristics of the Crab and Geminga pulsars

F. Aharonian[1], A.G. Akhperjanian[7], J.A. Barrio[2,3], K. Bernlöhr[1,8], H. Bojahr[6], J.L. Contreras[3], J. Cortina[3], A. Daum[1,10], T. Deckers[5], S. Denninghoff[2], V. Fonseca[3], J.C. Gonzalez[3], G. Heinzelmann[4], M. Hemberger[1,10], G. Hermann[1,11], M. Heß[1,10], A. Heusler[1], W. Hofmann[1], H. Hohl[6], D. Horns[4], A. Ibarra[3], R. Kankanyan[1], M. Kestel[2], O. Kirstein[5], C. Köhler[1], A. Konopelko[1], H. Kornmeyer[2], D. Kranich[2], H. Krawczynski[1,4], H. Lampeitl[1], A. Lindner[4], E. Lorenz[2], N. Magnussen[6], H. Meyer[6], R. Mirzoyan[2], A. Moralejo[3], L. Padilla[3], M. Panter[1], D. Petry[2,6,9], R. Plaga[2], A. Plyasheshnikov[1], J. Prahl[4], G. Pühlhofer[1], G. Rauterberg[5], C. Renault[1], W. Rhode[6], A. Röhring[4], V. Sahakian[7], M. Samorski[5], D. Schmele[4], F. Schröder[6], W. Stamm[5], H. Völk[1], B. Wiebel-Sooth[6], C. Wiedner[1], M. Willmer[5], H. Wirth[1]

[1] Max Planck Institut für Kernphysik, Postfach 103980, D-69029 Heidelberg, Germany
[2] Max Planck Institut für Physik, Föhringer Ring 6, D-80805 München, Germany
[3] Universidad Complutense, Facultad de Ciencias Físicas, Ciudad Universitaria, E-28040 Madrid, Spain
[4] Universität Hamburg, II. Institut für Experimentalphysik, Luruper Chaussee 149, D-22761 Hamburg, Germany
[5] Universität Kiel, Institut für Experimentelle und Angewandte Physik, Leibnitzstr. 15, D-24118 Kiel, Germany
[6] Universität Wuppertal, Fachbereich Physik, Gaußstr.20, D-42097 Wuppertal, Germany
[7] Yerevan Physics Institute, Alikhanian Br. 2, 375036 Yerevan, Armenia
[8] Now at Forschungszentrum Karlsruhe, P.O. Box 3640, D-76021 Karlsruhe, Germany
[9] Now at Universidad Autónoma de Barcelona, Institut de Física d'Altes Energies, E-08193 Bellaterra, Spain
[10] Now at SAP AG, Postfach 1461, D-69185 Walldorf, Germany
[11] Now at Enrico Fermi Institute, University of Chicago, 933 East 56th Street, USA

Received 13 Nov. 1998; Accepted 19 March 1999

Abstract. The Crab and Geminga pulsars were observed with the HEGRA stereoscopic IACT-System. A search for phase-resolved time structure of TeV gamma emission was carried out for both pulsars. No evidence for pulsed emission was observed. Geminga shows up as a TeV quiet object in our data. Upper limits were derived in units of the observed DC TeV Crab flux. The 3σ upper limit on DC TeV emission of Geminga is 13.0% of the Crab flux. Upper limits on pulsed emission were derived for the phase intervals which revealed pulsed emission in the EGRET 30 MeV - 10 GeV data. The 3σ upper limits on pulsed emission in these phase intervals are <2.3% and <7.2% of the Crab DC flux for the Crab and Geminga pulsars, respectively.

Key words: pulsars: individual: Crab and Geminga - gamma rays: observations

1. Introduction

The Crab and Geminga pulsars have both been extensively studied in wide ranges of the electromagnetic spectrum. The observations in the TeV energy domain are important in the context of supplying data at the highest photon energies currently accessible by experimental techniques. The angular resolution of imaging atmospheric Cherenkov telescopes (IACT's), which are today the most advanced detectors used for TeV gamma astronomy, is in the order of 0.1° for individual gamma-rays. This makes it still hard to distinguish between a pulsar and a nebula origin of the TeV-radiation on the basis of directional information[1] . Thus, the phase-resolved temporal analysis is currently the best method to obtain information on the correlation of TeV gamma rays with the pulsars.

1.1. The Crab pulsar

The 33 ms pulsed emission of the Crab pulsar is well established in most regions of the spectrum by various independent experimental observations. In fact, the pulsed emission observed by EGRET in 100 MeV - 10 GeV dominates the total emission in this energy domain, which is

Send offprint requests to: andreas.daum@sap-ag.de

[1] Note that also in the case of Geminga, there are indications of a surrounding nebula. X-ray observations with ASCA show diffuse emission extending to 0.3° around the pulsar (Kawai et al. 1998).

the adjacent domain to the TeV experiments. The observations performed by EGRET indicate a steepening of the spectrum of the pulsed emission at an energy $\approx$ 1GeV (Ramanamurthy et al. 1995). In addition, they indicate a harder spectrum of the unpulsed component compared to the pulsed component at energies greater than 1 GeV. The TeV observations reported in the past are contradictory. There are several reports of episodic pulsed emission (Gibson et al. 1982, Bhat et al. 1986, Acharaya et al. 1992) and persistent pulsed emission over a one year time interval (Dowthwaite et al. 1984). However, recent results of the Whipple IACT do not confirm the observation of pulsed TeV emission (Vacanti et al. 1992, Gillanders et al. 1997). In this paper we describe the analysis of HEGRA IACT system data of two observation periods. In terms of photon statistics and significance of the detected DC Crab emission, only the Whipple IACT data is competitive with data from the HEGRA IACT system.

1.2. The Geminga pulsar

The discovery of the pulsar nature of Geminga by ROSAT (Halpern et al. 1992) and the precise measurements carried out later by EGRET in the energy range between 30 MeV and 10 GeV demonstrate the ability to constrain emission models of pulsars by means of high energy observations. The 237 ms pulsed emission of Geminga is, in contrast to most other pulsars, not visible in most of the radio observations. The sole exception are observations at 102 MHz (Kuzmin et al. 1997); TeV observations would provide additional constraints on the physics of Geminga.

Traditional pulsar models predict cutoffs of the gamma ray radiation beyond 10 GeV, for a review see e.g. (Harding 1997). This would imply that only future ground based detectors, which will operate at 10 - 100 GeV, will be able to measure the turnover of the pulsar spectra and thus will provide information on the localization of the γ-ray production regions in the framework of these models. Indeed, despite several reports of possible detections of pulsed TeV radiation by the Tata group(Vishwanath 1993) and Durham group (Bowden 1993), observations with more sensitive imaging telescopes failed to confirm these early results (Akerlof 1993). The recent analysis of Geminga data taken by the Whipple observatory in Jan. 1997-March 1997 reports upper limits of 5.4% and 12.5% for the pulsed and DC emission flux level of Geminga compared to the Crab at energies greater than 300 GeV (Gillanders, priv. comm.).

However, recent developments of pulsar models predict the existence of a new component of γ-radiation with the interesting feature of a hard spectrum below 1 TeV and a sharp cutoff at $\approx$ 3 TeV (Romani 1996). Thus, a energy interval around 1 TeV is most promising for the detection of this component.

In the framework of this new model, the observational results obtained previously do not contradict as strongly as before, because the Tata and Durham group operate at threshold energies of 0.8 TeV and 1 TeV, respectively, whereas the Whipple observatory operates at $\geq$ 300 GeV. Furthermore, upper limits are usually derived assuming a spectrum model to account for energy dependencies of the experimental sensitivity. The assumption of a simple power law spectrum will bias the upper limits.

The HEGRA CT-System is currently the instrument with the best flux sensitivity in the 1-3 TeV energy band. Thus we tried to test the estimated flux of $1.5 \cdot 10^{-12}$ ph/cm^{2}s from Geminga between 1-3 TeV derived from the recent new model (Akerlof & Romani, priv. comm.), which does not contradict the Whipple upper limits. This flux level is only a factor of $\approx$10 below the flux F(E$\geq$1TeV) of the Crab and is detectable by the HEGRA CT-system within a few hours of data taking. The model predicts that more than half of the γ-ray flux is contained in less than 10% of the pulse phase, a feature which would ease a detection.

2. The HEGRA IACT System

The HEGRA IACT System is located on the Canary island of La Palma. A detailed description of the IACT system is provided in (Daum et al. 1997a, Daum & Hermann 1997, Daum 1997). The purpose of the system is the stereoscopic observation of air showers induced by primary cosmic particles in the TeV energy domain. The HEGRA IACT system is the first detector which makes routinely use of the stereo-imaging technique (Aharonian 1993, Kohnle et al. 1996, Ulrich et al. 1998). The unique features of an IACT system are exploited already at the trigger level (Daum et al. 1997b, Bulian et al. 1998), where a remarkable reduction of background arising from night sky background illumination can be achieved. Also, the background due to Cherenkov light emitted from local muons is virtually eliminated, which for single dish experiments in the energy range below 1 TeV otherwise represents a crucial background.

The primary benefit of the stereoscopic technique is the unambiguous reconstruction of the geometry of the air shower. The determination of the geometrical parameters not only results in a precise angular reconstruction of the primary particle's direction of origin (Pühlhofer et al. 1997) but also enables a precise measure of the energy (Hofmann 1997, Aharonian et al. 1998) and improves the determination of the nature of the primary particle.

With these features, the HEGRA IACT system is one of the most sensitive and accurate experimental instruments for ground based TeV gamma astronomy currently operating.

3. Reconstruction of the parameters of the primary particle

The analysis of data registered with the HEGRA IACT system experiment follows the techniques described in detail in (Daum et al. 1997a). Only the level of tail cuts applied for the preparation of images varies depending on the hardware used during certain observation periods. The values chosen are listed further below in the observation sections.

3.1. Direction of origin

The angular resolution of individual primary TeV gamma-rays is of the order of 0.1° with an absolute pointing error of 0.01°. It is achieved by the stereoscopic imaging analysis of individual events and additional calibration data which supplies information on the absolute pointing of the telescopes (Pühlhofer et al. 1997).

3.2. Gamma/hadron separation

The trigger condition of two neighbored pixels in a camera and the two-telescope coincidence already suppresses hadronic events at the trigger level. For the study of point sources, the angular resolution described above is used to reduce the backgrounds by another factor of $\approx$100. Further suppression is achieved by cuts exploiting the shape of Cherenkov images.

The actual image parameters of individual events are compared to the distributions (e.g. probability density functions) which are obtained by Monte-Carlo simulations (Konopelko et al. 1998). In the analysis of Geminga data a set of tight shape cuts (Daum et al. 1997a) is used for the search for TeV gamma-rays under "background free" conditions. These tight cuts reduce the hadron background by an additional factor of $\approx$ 100 whereas a gamma efficiency of up to 40% (in the case of a 4 telescope system) is maintained. In the Crab data analysis, where the well known "background" of a persistent DC TeV gamma-ray emission (Weekes et al. 1989, Vacanti et al. 1991, Goret et al. 1993, Baillon et al. 1993, Tanimori et al. 1994, Konopelko et al. 1996) has to be dealt with, a loose shape cut with "mean scaled width" < 1.3 is applied (Aharonian et al. 1997). In this case the hadron reduction factor is $\approx$ 3 with a gamma efficiency $\geq 80\%$. The resulting high statistics of TeV gamma-rays is needed for the precise determination of the flux of the DC emission. This DC emission plays the role of a well determined "background" in the search for additional pulsed emission.

3.3. Energy reconstruction

The reconstruction is based on the dependence of the expected number of photoelectrons per telescope image, the so-called *size*, on the distance r of the telescope from the shower axis, on the primary photon energy E and on the zenith angle Θ. The mean and variance of the *size* are computed from Monte Carlo event-samples for bins in r, E and Θ. Polynomial fits are used to interpolate between bins. For each event an energy estimate E_i of an individual telescope is obtained by inverting the $size(E, r, \Theta)$-relation. The reconstructed geometrical shower parameters are used to estimate r and are thus essential for the method. Subsequently the energy estimates E_i of all telescopes with good images are combined by calculating a weighted mean energy (Aharonian et al. 1998 and Köhler 1998). Because this analysis does not focus on the precise determination of spectra, only loose additional requirements were imposed in order to keep the experimental TeV photon statistics. At least one telescope with $r_i < 200$ meters and a reconstructed shower zenith angle less than 45° was required. Detailed spectral analyses use additional cuts, see (Aharonian et al. 1997, 1998). This energy reconstruction yields a resolution of ΔE/E$\leq$25%.

3.4. Pulsar phase-resolved reconstruction of TeV gamma-ray timing

In order to perform a phase-resolved timing study of millisecond pulsars, one needs a (redundant) experimental time measurement with a precision better than a millisecond and an algorithm for the transformation of event times to the rest frame of the pulsar. For most single pulsars, the transformation to the solar system barycenter is sufficient (Backer et al. 1986, Taylor et al. 1989, Bell 1996).

Since the beginning of the HEGRA experiment in 1989 an atomic clock and a GPS receiver were operated (see Merck 1993). The time tags of this atomic clock and the GPS receiver are recorded for each event to an accuracy of 200 ns.

For the transformation of the event times to the solar system barycenter the DE200/LE200 ephemerides (Standish 1982) were used to derive one set of data for each day at midnight[2]. The set contains the geocenter position, velocity, acceleration and the time-derivative thereof plus the sun's position relative to the SSB. The accuracy of the earth's position in this dataset is of the order of 200 meters and thus the timing error well below 1 millisecond. By using a Taylor expansion, the vector from the geocenter to the SSB can be calculated for any time.

In order to perform phase-resolved studies, one needs additional information on the pulsar time structure. For

[2] This dataset was produced by L.Norci, MPI für Extraterrestrische Physik , Garching.

most pulsars this data can be obtained from the Princeton Pulsar Group (Princeton WWW, Arzoumanian et al. 1992). In the case of the Crab Pulsar, redundant information can be obtained from the Nuffield Radio Astronomy Laboratories - Jodrell Bank (Lyne A.G. & Pritchard 1998). In Sect. 4 and Sect. 5 we present the used parameters in detail.

4. Observations of the Crab

The data analyzed in this work were taken during the two seasons 1996/1997 and 1997/98. In the season 1996/97 the observations were performed in the traditional ON-OFF manner (Daum et al. 1997a). In 1997/98 the so called "wobble mode" was used (see Aharonian et al. 1997 for details on this observation mode).

The various data sets differ slightly in terms of the experimental hardware and, as a result, of the software analysis parameters. Table 1 summarizes the experimental conditions for the different data sets. In autumn 1996 the HEGRA CT-system was still at an interim stage concerning the number of operational telescopes, readout electronics and trigger conditions. In autumn 1997 the CT4 was out of service for some weeks due to a fire at the HEGRA experimental site. In the software analysis different tail cuts were applied. In the case of the initial 40 MHz FADC readout a two level tail cut of 7/8 p.e. was used. Later on, a 120 MHz FADC was used and the tail cuts were lowered to 3/6 p.e. as in (Daum et al. 1997a). The single pixel trigger threshold was lowered after Period 56 from 8 to 7 photo electrons.

The total time of observations under stable hardware and good weather conditions is ≈83 hours. During 70 hours the zenith angle was lower than 45 degrees. This data subset is used in the analysis involving the energy reconstruction of the primary photon.

The software analysis includes a gamma/hadron separation cut discussed in section 3.2, *mean scaled width* < 1.3. Fig. 1 shows the TeV gamma-ray signal observed from the Crab as a function of Θ^2, the square of the angular deviation between the reconstructed direction of the shower and the Crab coordinates. A directional selection $\Theta^2 < 0.017\ deg^2$ was applied, corresponding to a maximum deviation of 0.13 degrees. This is the optimum cut for point sources taking into account the point spread function of the HEGRA 4-CT-system (Daum et al. 1997a, Pühlhofer et al. 1997). After all cuts, 6007 events in the ON observations and 2987 events in OFF-sample remain, reflecting a detection at the 32σ level and implying the possibility of splitting up the data into several subsamples without loosing the ability of significant detection of TeV emission in the subsamples. In order to improve the background statistics for the subsequent timing analysis, the background region was enlarged to $\Theta^2 < 0.34\ deg^2$, which results in a factor of 20 more statistics. This field of

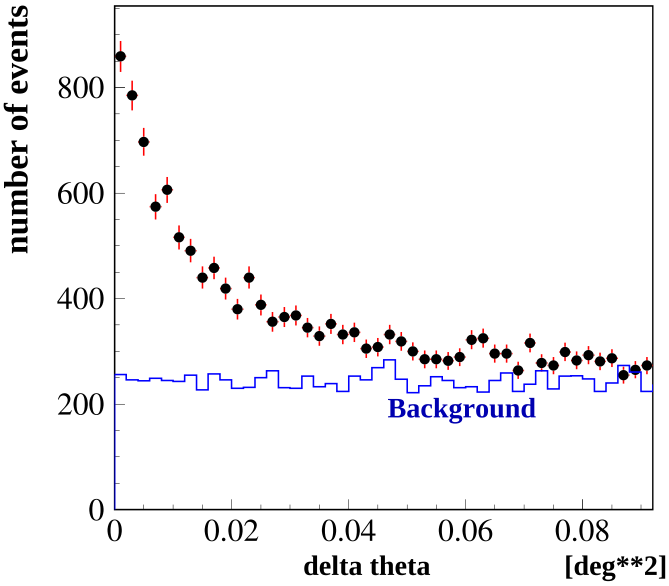

Fig. 1. Observed number of events as a function of the square of the angular deviation of the reconstructed direction of origin of a photon relative to the Crab pulsar. The background is derived from OFF source observations.

0.58 degree radius is small compared to the field of view of the HEGRA telescope cameras and is inside the region of flat sensitivity of the instrument.

Given the non-uniform experimental data set, it was necessary to produce several different Monte Carlo (MC) event samples which reflect the various experimental conditions. These MC samples are then weighted by taking into account the zenith-angle dependent observation time of each observation period. Simulations with $0°, 20°, 30°$ and $45°$ observation zenith angle were used. The distribution in zenith angle of the total observation time and the energy-dependent effective detection area, after all cuts including the energy reconstruction, is derived from the simulations and shown in Fig. 2.

The energy reconstruction is performed using the appropriate MC event samples and applying the method previously explained. Fig. 3 shows the differential energy spectrum of the experimental data and the MC-spectrum for a power-law input spectrum, with an index and normalization chosen to fit the data. The integral flux above 1 TeV of $F(E \geq 1TeV) = 1.42 \pm 0.04(\mathrm{stat.})10^{-11}\mathrm{ph/cm^2s}$ shows good agreement with recent measurements undertaken by other groups (Carter-Lewis et al. 1997). A detailed description of the precise determination of the Crab energy spectrum will be given elsewhere(Konopelko, in prep.). In the context of this analysis, the energy reconstruction is primarily used to divide the total data into two samples, $>$ 1TeV and $<$1TeV primary energy, in order to perform a search for pulsed TeV emission of the Crab in the total event sample and in two distinct en-

Table 1. Summary of experimental data sets . The new-moon periods in the 1st column are denoted by PN, were N=1 was the first new-moon observation period of HEGRA CT1 in 1992. The 3rd column lists identification numbers of the telescopes operating in the system. Please note that at the HEGRA experiment there exist in total 6 telescopes, but currently only telescope 3-6 belong to the CT-system. The 4th column denotes the FADC frequencies used in the different telescopes, which affects the effective integration time and thus the noise due to background light. The 5th column lists the single pixel trigger threshold in units of photoelectrons.

Period	date	active CT's	FADC ν [MHz]	trigger thr	obs. time
P52-54	Sep-Nov 1996	3,4,5	120,40,40	8.p.e.	11.3 h
P55-56	Dec'96-Jan'97	3,4,5,6	all 120	8.p.e.	5.4 h
P64	Aug/Sep 1997	3,4,5,6	all 120	7.p.e.	10.0 h
P66	Oct/Nov 1997	3,5,6	all 120	7.p.e.	14.2 h
P67a	Nov 1997	3,5,6	all 120	7.p.e.	3.4 h
P67b	Nov/Dec 1997	3,4,5,6	all 120	7.p.e.	4.4 h
P68	Dec'97-Jan'98	3,4,5,6	all 120	7.p.e.	12.0 h
P69	Jan 1998	3,4,5,6	all 120	7.p.e.	22.2 h

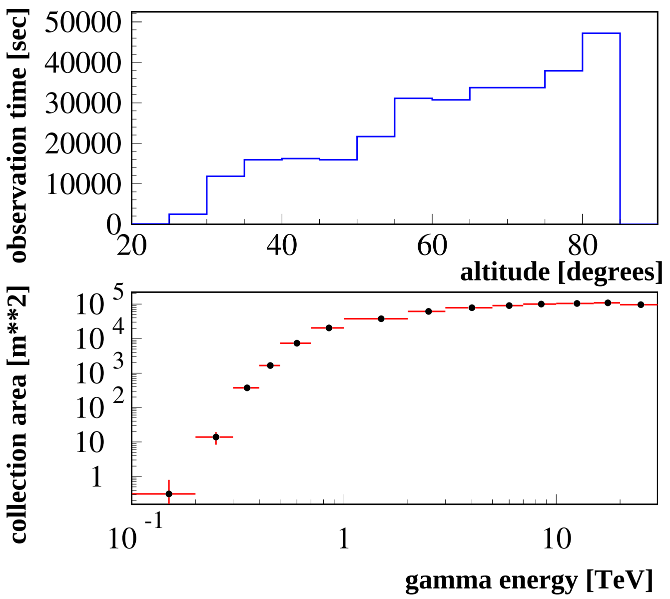

Fig. 2. Upper plot: Observation time for the Crab Nebula, for different bins in altitude. Lower plot: effective area derived from Monte Carlo event samples reflecting the various experimental conditions. The different experimental conditions are weighted with the experimental observation time.

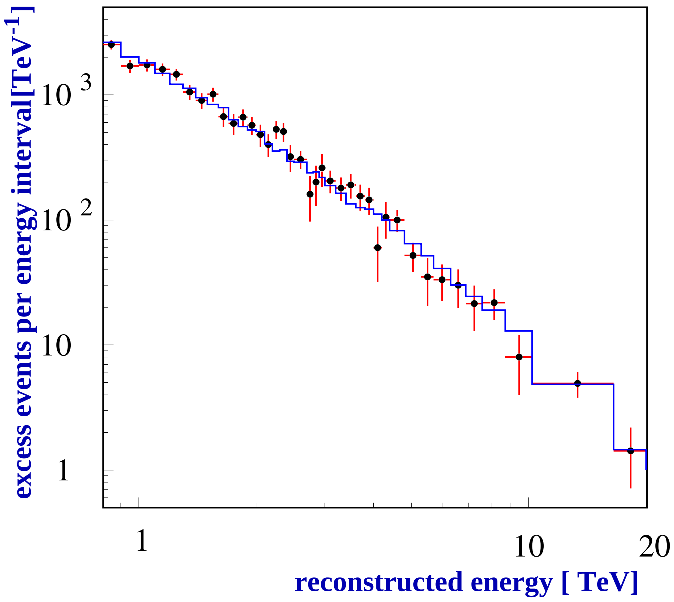

Fig. 3. Dots with error bars: Differential energy spectrum as observed from the Crab. Histogram: Monte Carlo energy spectrum derived from a 2-parameter fit of a forward folded power law spectrum, in the same energy bins as the data.

ergy ranges. In addition, one can search for pulsar-phase dependent changes in the spectral index.

The reconstruction of the pulsar phase of events was based on the Crab pulsar timing data base of Jodrell Bank, because of the faster availability of this data. This data base is updated regularly each month. The radio timing parameters used for the Taylor expansion $\Phi(T)$ (see Eq. (1)) are listed in Table 2.

$$\Phi(T) = \Phi(T_0)+f_0(T-T_0)+\frac{1}{2}f_1(T-T_0)^2+\frac{1}{6}f_2(T-T_0)^3 \quad (1)$$

The observed number of events from the direction of the Crab Nebula is shown in Fig. 4, as a function of the pulsar phase. The distributions of all data and of the subsamples E_γ >1TeV and E_γ <1TeV are statistically consistent with a uniformly distributed gamma-ray emission, with respect to the Crab Pulsar phase. Also the data subsamples of the several observation periods (see Table 1) show no outstanding episodic pulsed emission of the Crab.

A quantitative analysis of upper limits on pulsed TeV emission was performed by testing a model of persistent pulsed TeV emission. Given the observations in the adjacent experimental energy domain (30 MeV - 10 GeV) by EGRET (Fierro et al. 1998), which show a main pulse in the phase interval [-0.06,0.04] around the time of the main radio pulse, a 10% duty cycle centered on the radio

Table 2. Radio timing parameters of the Crab Pulsar . The integer part of $t_{0,geo}$ denotes the barycentric epoch (TDB) of f0,f1,f2. The remaining fraction denotes the geocentric arrival time of a pulse (corrected for infinite observation frequency).

validity [MJD]	$t_{0,geo}$ [MJD]	f0 [s^{-1}]	f1 [s^{-2}]	f2 [s^{-3}])
50327-50356	50341.000000162	29.8851450044842	-3.75680e-10	0.00e+00
50357-50387	50372.000000118	29.8841388046120	-3.75671e-10	0.00e+00
50388-50417	50402.000000312	29.8831651355263	-3.75623e-10	1.14e-20
50418-50449	50433.000000282	29.8821591154998	-3.75592e-10	0.00e+00
50449-50479	50464.000000371	29.8811532491936	-3.75565e-10	-1.30e-19
50662-50691	50676.000000124	29.8742757674534	-3.75377e-10	1.46e-20
50692-50721	50706.000000134	29.8733028378748	-3.75349e-10	1.05e-20
50722-50743	50732.000000006	29.8724596777066	-3.75338e-10	1.05e-20
50744-50790	50769.000000071	29.8712598955826	-3.75290e-10	1.05e-20
50783-50813	50797.000000352	29.8703520237117	-3.75270e-10	2.23e-22
50814-50844	50829.000000345	29.8693145331841	-3.75266e-10	7.21e-20

pulse was assumed[3]. This is the interval [-0.05,0.05] of the distributions shown in Fig. 4. All three ON distributions as well as the background are statistically consistent with a constant.

The upper limit is derived by measuring the level of the DC TeV gamma emission and calculating the ratio R of pulsed/DC emission in one step:

$$R = \frac{P - \frac{1}{9}DC}{\frac{10}{9}(DC - DB)} \tag{2}$$

with
P:= ON observation counts in [-0.05,0.05] phase interval
DC:= ON observation counts outside the above interval
DB:= Background outside the above interval

Thus, the upper limits expressed in terms of the observed persistent DC emission are unaffected by possible systematic errors in the determination of the effective area[4]. The final calculation of the upper limit also takes into account our experimental error of the measurement of the DC emission. Systematic errors on the absolute energy scale, which are today still the major source of systematics in the flux determination by Cherenkov telescope experiments are in the order of 15% for the HEGRA system (Fraß et al. 1997). They enter the analysis only as a shift of the borders of the energy-selected subsamples.

The error ΔR on R is calculated by Gaussian error propagation. By using R,ΔR and the method of (Helene 1983), 3σ (99.865% C.L.) upper limits are derived and listed in Table 3. Note that the maximum counting rate of this data sample is observed at $\approx$ 0.8TeV, thus determining the low energy boundary (see also the effective area in Fig. 2). The high energy boundary of 20 TeV is determined by the ability of a significant DC detection (see Fig. 3).

Table 3. Upper limits on the ratio R of pulsed/DC TeV gamma emission of the Crab assuming a 10% duty cycle centered on the radio pulse timing .

Energy region	U.L. on pulsed emission [% of DC]
no energy selection	2.3
$E_\gamma < 1TeV$	5.7
$E_\gamma > 1TeV$	3.3

The quoted upper limits can be converted into absolute flux limits by taking into account an absolute Crab DC flux.

The spectral index of pulsed and DC emission may not be identical. If there are extreme differences in the spectral slope of the pulsed and DC emission, the pulsed emission may show up first as a dependence of the spectral index on the rotational phase of the pulsar. By comparing the measured spectral slopes of several pulsar phase subsamples to the slope at phase=0.0 (this is the phase of the main EGRET and radio pulse), the experimental systematic errors of the energy reconstruction cancel. In the energy range 0.8-20 TeV twenty fits equivalent to that shown in Fig. 3 were performed. The differences of the spectral indices to the mean index measured in the phase region [-0.05,0.05] were computed. Fig. 5 shows the variation of the spectral index as a function of the pulsar phase. Fitting a constant distribution with subsequent analysis of the χ^2 yields a $\approx$70% probability of constant indices. Given these results, a correlation analysis of pulsar phase dependent spectral slopes with the EGRET observations (Fierro et al. 1998) was omitted.

5. Observations of Geminga

The data analyzed here were taken from Jan. 15 - 25, 1998 in the so called "wobble mode". The total time of

[3] In addition, there exists a less prominent pulse at phase$\approx$0.4 in the EGRET data.

[4] Note that the upper limit analysis discussed here implicitly assumes an identical spectrum of the pulsed and DC emission. Different spectral indices affect the experimental sensitivity and thus create systematic errors on the ratio R.

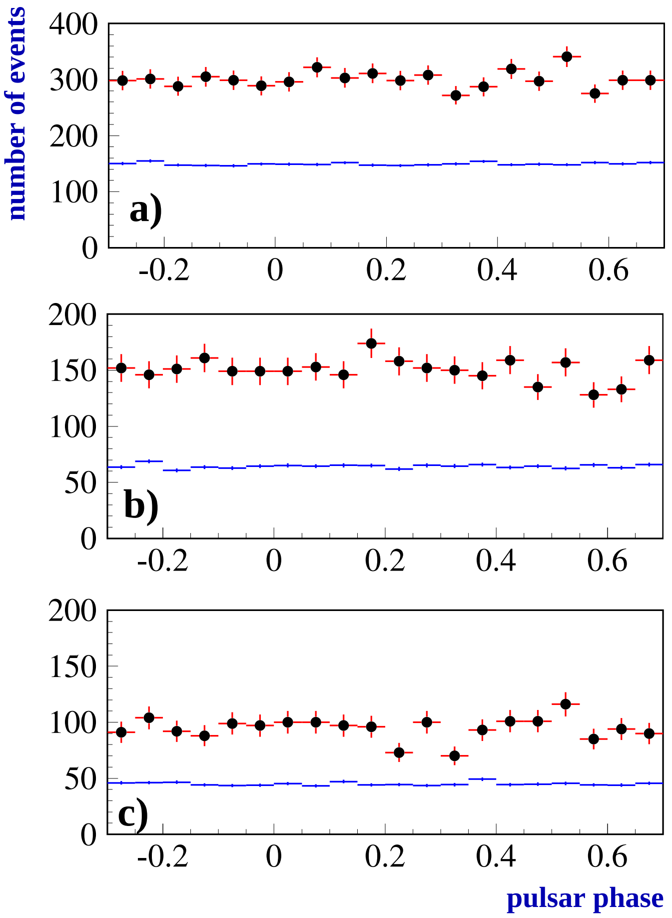

Fig. 4. Observed number of events from the direction of the Crab as a function of the Crab pulsar phase. The dots with error bars are ON observations, the lower histograms are background estimates derived from OFF observations with extended angular acceptance. a) total data sample; b) reconstructed primary energy <1TeV; c) reconstructed primary energy >1TeV.

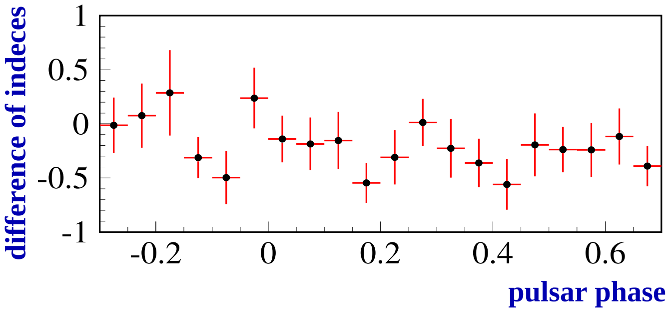

Fig. 5. Difference of spectral indices as derived from 2-parameter (normalization and spectral index) power law fits to pulsar-phase dependent subsets of Crab observation data. The spectral indices are referred to the mean index observed in the interval [-0.05,0.05].

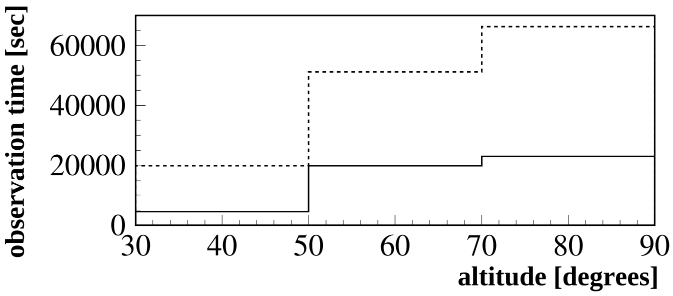

Fig. 6. Altitude dependent observation time of Geminga (full line) and the Crab data of P67b,P68,P69.

observation with stable hardware and good weather conditions was ≈13 hours. The data was taken under the same hardware conditions as the Crab data of the observation periods P67b,P68,P69 (Nov.1997 to Jan. 1998, see Table 1). This Crab data is used as a reference in the subsequent analysis, taking into account the altitude-dependent observation times of Crab and Geminga[5]. Fig. 6 shows the observation time of Geminga and of the Crab sample, as a function of altitude. First, the distribution of events was studied as a function of the reconstructed direction of origin relative to the Geminga pulsar. Fig. 7 shows the observed distributions after applying loose and tight gamma/hadron separation cuts. No obvious TeV gamma emission is revealed in these plots, in contrast to the Crab observation shown in Fig. 1. Consequently, an upper limit on pulsed TeV emission from the Geminga pulsar is derived based on the assumption of zero DC emission. In contrast to the Crab analysis, in this case there is no need for a precise determination of the DC flux level by high photon statistics. Tight gamma/hadron separation cuts and a directional selection adapted to the point-spread function of the 4-CT system yield best flux sensitivity for small flux values, well below the Crab flux.

In order to reconstruct pulsar-phase resolved event times, the SSB transformation was applied by using the pulsar timing data base listed in Table 4. From the Princeton Pulsar data base (Princeton FTP) the $t_{0,geo}$ data was obtained which describes the absolute phase at the given epoch. This ephemeris data was also used for the phase-resolved analysis of the EGRET data (Fierro et al. 1998). It is the outcome of a "Z_n^2 timing method" based on the first four years of EGRET observations (Mattox 1994, Fierro et al. 1998). The quoted time of validity extends from MJD 47715-50197. The second derivative is measured with an upper limit of $f2 < 6 * 10^{-24}$ and is set to zero. Fortunately, more precise measurements of the Geminga ephemeris have been published recently (Mattox et al. 1998). This ephemeris data was obtained by a combined data analysis of SAS2,COSB and EGRET data of a time span of 24 years from year 1973.0 until 1997.2. No glitch was observed in that data and a 3rd order Taylor expansion describes the whole dataset. The authors quote

[5] Note that the sensitivity of the instrument shows altitude dependencies, especially in the case of tight gamma/hadron separation cuts.

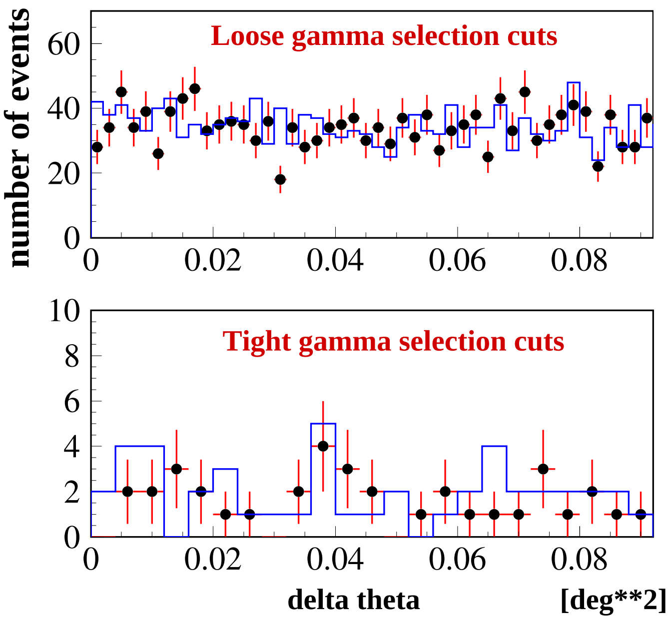

Fig. 7. Number of events as a function of the square of angular deviation of the reconstructed direction of origin with respect to the Geminga pulsar. Upper plot: after loose gamma/hadron separation ("scaled width < 1.3"); lower plot: after applying tight gamma/hadron separation.

Table 4. Geminga Pulsar timing parameters used in this analysis. The first line is used for the determination of the absolute phase at a given epoch ($t_{0,geo}$). The second line ephemeris with epoch MJD=46599.5 is used for the Taylor expansion $\Phi(T)$.

$t_{0,geo}$ [MJD]	f0 $[s^-1]$	f1 $[s^-2]$	f2 $[s^-3]$)
48750.000001780	4.2176690940300	-1.95206e-13	0.00D-25
	4.217705363081	-1.9521712e-13	1.49e-25

an accuracy of the pulsar phase description better than 100 milliperiods until year 2008, if no glitch will occur. This precise ephemeris data (see Table 4) was used for the calculation of the Taylor expansion $\Phi(T)$. The $t_{0,geo}$ data served for the determination of the absolute phase, thus enabling us for a direct comparison to the phase analysis of EGRET data (Fierro et al. 1998). Fig. 8 shows the phase-dependent event times of Geminga after tight gamma/hadron selection. This histogram is used for the following calculation of upper limits.

The observations by EGRET in the adjacent energy band 20 MeV - 10 GeV show two prominent peaks P1[0.62,-0.71] and P2[0.09,0.22]. Motivated by these observations, a double-peaked pulsed emission in the TeV energy band with P1[0.6,0.7] and P2[0.1,0.2] was considered in the upper limit analysis.

The upper limit on pulsed TeV gamma emission of the Geminga pulsar in the P1+P2 phase intervals is derived by Eq. (3). Tight gamma/hadron separation cuts and a directional selection $\Theta^2 < 0.017deg^2$, which is adapted to the point-spread function of the CT-system, were applied.

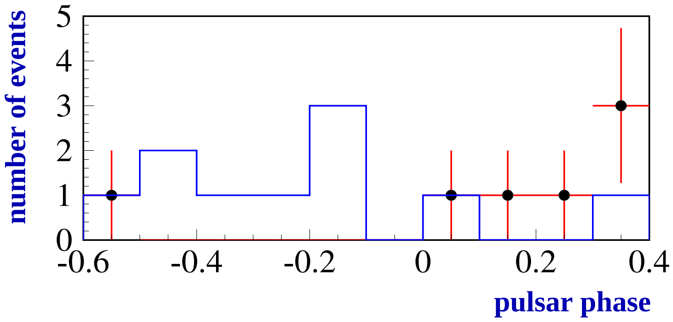

Fig. 8. Observed number of events after tight gamma/hadron selection from the direction of the Geminga pulsar depending on the Geminga pulsar phase. The dots with error bars are ON observations, the histogram is a background estimate from OFF regions.

The 99.865% C.L. lower limit of background events was calculated by using Poisson statistics and taking the actual measured number as an estimate of the mean of the Poisson distribution. This leads in all cases to a lower limit of zero background, except in the case of the analysis without energy selection, where the lower limit of the DC Geminga OFF observation (DCOFF) is 2. In the case of the pulsed analysis, the background is calculated by scaling the total background with the duty cycle of the assumed emission. This results in a background L.L. for the pulsed analysis without energy selection of 0.4 events. Thus, the background taken into account for the analysis was set to zero events. The number of excess events is determined by the number of ON counts minus the previously discussed lower limit of background. The 99.865% upper limit on this number of excess events is determined by a Poisson distribution that matches the requirement that the integrated probability of having less or equal the actual number of excess events is $\leq 0.135\%$. The expectation value of this Poisson distribution is taken as upper limit on the number of excess events.

The U.L. of excess events is related to the 3σ lower limit of expected excess events for a Crab flux level. This expected number is derived from the Crab measurements by weighting them with the zenith angle dependent observation time relative to the Geminga observations. The error is derived by Gaussian error propagation. The number of events used for the calculation of upper limits are listed in Table 5.

$$R = \frac{U.L.\ (excess\ events)}{Crab\ L.L.} \tag{3}$$

with
U.L. (excess events) as derived from Poisson statistics
CRAB L.L.= expected Crab excess - 3 * σ(thereof)

The upper limits of TeV emission from Geminga derived by Eq. (3) are listed in Table 6. In order to divide the total Crab excess event sample into two equally large samples, a cut at 1.5 TeV is used. The application

Table 5. Number of events obtained in the Geminga analysis and used for the calculation of upper limits by Eq. (3). The last column shows the number of excess events expected from the Crab analysis for a flux level equal to that of the Crab .

Energy region	DC ON	P1+P2 ON	DC OFF	Crab
no E_γ selection	7	1	10	145.1±7.43
$E_\gamma < 1.5TeV$	3	1	5	59.57±4.77
$E_\gamma > 1.5TeV$	2	0	2	71.00±5.13

Table 6. Upper limits on the TeV emission of Geminga in units of Crab DC emission flux . The pulsed emission is assumed to be double-peaked on the phase intervals P1[0.6,0.7] and P2[0.1,0.2] which coincide with the pulses observed by EGRET. Upper limits on DC emission of Geminga are shown in the 3rd column.

Energy region	U.L. pulsed [Crab DC]	U.L. DC [Crab DC]
no energy cut	7.2%	13.0%
$E_\gamma < 1.5TeV$	19.7%	27.8%
$E_\gamma > 1.5TeV$	11.9%	19.4%

of tight gamma/hadron selection cuts shifts the accepted spectrum towards higher energies (compared to the loose selection used in the Crab analysis). In addition to the pulsed emission U.L. also a persistent DC emission was considered.

These upper limits in terms of Crab flux units are valid under the assumption of a spectral index equal to that of the Crab TeV emission.

6. Summary and discussion

The HEGRA IACT system data of Crab observations reveals a highly significant detection of the TeV DC emission with high photon statistics. This allowed us to study the pulsar-phase dependent characteristics with high precision. Neither the flux level nor the spectral index show a statistically significant modulation with the pulsar phase. Models of the Crab, which support persistent pulsed TeV emission greater than a few percent of the DC emission, are ruled out. No outstanding episodic pulsed emission of the Crab is observed in the HEGRA CT system data.

The observational results of the Geminga pulsar do not reveal any significant TeV gamma emission. This is also the case for the phase-resolved analysis, which is more sensitive than the DC analysis because of the improved signal-to-noise ratio. The upper limits at the level of few percent of the Crab DC flux are still consistent with the recent estimates of $\approx 5\%$ pulsed and $\approx 10\%$ total emission flux of the Crab DC flux F(E≥1 TeV) (see Sect. 1) in the energy interval 1-3 TeV.

Acknowledgments

The support of the German Ministry for Research BMBF and of the Spanish Research Council CYCIT is gratefully acknowledged. We thank the Instituto de Astrofisica de Canarias for the use of the site and for providing excellent working conditions. We gratefully acknowledge the technical support staff of Heidelberg, Kiel, Munich, and Yerevan. We thank A.Lyne and B.Pritchard (NRAL) for the private communication on Crab ephemeris data. We gratefully acknowledge the private communication with R.Romani who supplied us with estimates on the TeV γ-ray flux of Geminga. We thank G.H. Gillanders for privately informing us about the results of the analysis of Geminga data taken by the Whipple observatory.

References

Acharaya B.S., Bhat P.N., Gandhi V.N., et al., 1992 , A&A 258, 412
Aharonian F., 1993 , Proceedings of the Int. Workshop "Towards a Major Atmospheric Cherenkov Detector II", Calgary, R.C. Lamb (Ed.), 81
Aharonian F., Akhperjanian A.G., Barrio J.A., et al., 1997 , A&A 327, L5-L8
Aharonian F., Akhperjanian A.G., Barrio J.A., et al., 1998 , accepted by A&A
Akerlof C.W., Breslin A.C., Cawley M.F., et al., 1993 , A&A 274, L17.
Arzoumanian Z., Nice D., Taylor J. H., 1992 , GRO/radio timing data base, Princeton University
Backer D.C. , Hellings R.W., 1986 , ARAA 24 , 537
Baillon P., Behr L., Danagoulian S., et al., 1993 , Astroparticle Phys. 1, 341
Bell J., 1996, course on "Introduction to Pulsar Astronomy", http://www.jb.man.ac.uk/ pulsar/Education/Tutorial/tut/tut.html
Bhat P.N., Ramanamurthy V., Sreekantan B.V., et al., 1986 , Nat 319, 127
Bowden C.C.G., Bradbury S.M., Chadwick P.M., et al., 1993 , J.Phys. G 19, L29.
Bulian N., Daum A., Hermann G., et al., 1998 , Astroparticle Phys. 8, 223
Carter-Lewis D.A., Biller S., Boyle P.J., et al., 1997 , Proc. 25th ICRC, Durban, South Africa, Vol. 3, OG, 161
Daum A., 1997 , Proc. 25th ICRC, Durban, South Africa, Vol. 5, OG, 121
Daum A., Hermann G., 1997 , Proc. 25th ICRC, Durban, South Africa, Vol. 5, OG, 117
Daum A., Hermann G., Heß M., et al., 1997a , Astroparticle Phys. 8, 1
Daum A., Hermann G., Heß M., Rauterberg G., 1997b , Proc. 25th ICRC, Durban, South Africa, Vol. 5, OG, 129
Dowthwaite J.C., Harrison A.B., Kirkman L.W., et al., 1984 , ApJ 286, L35
Fierro J.M., Michelson P.F., Nolan P.L., 1998 , ApJ 494, 734
Fraß A., Köhler C., Hermann G., et al., 1997 , Astroparticle Phys. 8 , 91

Gibson A.L., Harrison A.B., Kirkman L.W., et al., 1982 , Nat 296, 833

Gillanders G.H., Boyle P.J., Buckley J.H., et al., 1997 , Proc. 25th ICRC, Durban, South Africa, Vol. 3, OG, 185

Goret P., Palfrey T., Tabary A., et al., 1993 , A&A 270, 401

Halpern J.P., Holt S.S., 1992 , Nat 357, 222

Harding A.K., 1997 , Astr. Soc. Pacific Conf. Ser., in press.

Helene O., 1983 , Nucl. Instr. and Methods, 212, 319

Hofmann W. , 1997 , Proc. of Kruger National Park Workshop on TeV Gamma-Ray Astronomy "Towards the Major Cherenkov Detector - V", South Africa

Kawai N., Tamura K., Shibata S., 1998 , "X-ray pulsar Nebulae", Proc. "Neutron Stars and Pulsars", Ed. N.Shibazaki et al., Universal Academy Press, Tokyo, 449

Köhler C., 1998 , PhD thesis Universität Heidelberg

Kohnle A., Aharonian F., Akhperjanian A., et al., 1996 , Astroparticle Phys. 5, 119

Konopelko A., Aharonian F., Akhperjanian A., et al., 1996 , Astroparticle Phys. 4 , 199

Konopelko A.K., Hemberger M., Aharonian F., et al, 1998 , "Performance of the Stereoscopic System of the HEGRA Imaging Air Cherenkov Telescopes", submitted to Astroparticle Phys.

Kuzmin A.D., Lovosky B. Ya., 1997, IAU Circ. No. 6559

Lyne A.G., Pritchard R.S., 1998 , http://www.jb.man.ac.uk/ pulsar/crab.html

Mattox J.R., 1994 , in "The Second Compton Symposium", AIP Conf.Proc., 304

Mattox J.R, Halpern J.P., Caraveo P.A., 1998 , ApJ 493, 891

Merck M., 1993 , PhD thesis Universität München

Princeton Pulsar Group, http://pulsar.princeton.edu/

Princeton Pulsar Group, anonymous ftp puppsr.princeton.edu (128.112.128.165) and therein /gro/psrtime.dat

Pühlhofer G., Daum A., Hermann G., et al., 1997 , Astroparticle Phys. 8, 101

Ramanamurthy P.V., Bertsch D.L., Fichtel C.E., et al., 1995 , ApJ 450, 791

Romani R., 1996 , ApJ 470, 469

Standish E.M., 1982 , A&A 114 , 297

Tanimori T., Tsukagoshi T., Kifune T., et al., 1994 , ApJ 429, L61

Taylor J.H., Weisberg J.M., 1989 , ApJ 345, 434

Ulrich M., Daum A., Hermann G., Hofmann W., 1998 , J. Phys. G 24 , 883

Vacanti G., Vawley M.F.C., Colombo E., et al., 1991 , ApJ 377, 467

Vacanti G., 1992, ApJ 377, 467

Vishwanath P.R., Sathyanarayana G.P., Ramanamurthy P.V., et al., 1993 , A&A 267, L5

Weekes T.C., Cawley M.F., Fegan D.J., et al., 1989 , ApJ 342, 379